Linearized semiclassical initial value time correlation functions using the thermal Gaussian approximation: Applications to condensed phase systems

Jian Liu and William H. Miller

Department of Chemistry and K. S. Pitzer Center for Theoretical Chemistry

University of California,

and Chemical Science Division, Lawrence Berkeley National Laboratory

Berkeley, California 94720-1460

Abstract

The linearized approximation to the semiclassical initial value representation (LSC-IVR) has been used together with the thermal Gaussian approximation (TGA) (TGA/LSC-IVR) [J. Chem. Phys. **125**, 224104 (2006)] to simulate quantum dynamical effects in realistic models of two condensed phase systems. This represents the first study of dynamical properties of the Ne_{13} Lennard-Jones (LJ) cluster in its liquid-solid phase transition region (temperature from 4 K to 14 K). Calculation of the force autocorrelation function shows considerable differences from that given by classical mechanics, namely that the cluster is much more mobile (liquid-like) than in the classical case. Liquid *para*-hydrogen at two thermodynamic state points (25 K and 14 K under nearly zero external pressure) has also been studied. The momentum autocorrelation function obtained from the TGA/LSC-IVR approach shows very good agreement with recent accurate path integral Monte Carlo (PIMC) results at 25 K [J. Chem. Phys. **125**, 024503 (2006)]. The self-diffusion constants calculated by the TGA/LSC-IVR are in reasonable agreement with those from experiment and from other theoretical calculations. These applications demonstrate the TGA/LSC-IVR to be a practical and versatile method for quantum dynamics simulations of condensed phase systems.

I. INTRODUCTION

Theoretical simulations of the dynamics of large molecular systems is an extremely active area of research nowadays, and as in most areas of theory, the accuracy of the treatment is inversely related to the ease of its application. It is thus useful to have a full 'menu' of theoretical approaches, from the very accurate, which may be difficult to apply to very large systems, to much simpler and more approximate methods that are more readily applicable to complex molecular systems.

Perhaps the simplest theoretical approach to chemical dynamics is classical mechanics, i.e., classical molecular dynamics (MD) simulations (which are extremely wide spread nowadays), while the most accurate treatment is of course a complete solution of the time-dependent Schrödinger equation. Semiclassical (SC) theory[1,2] stands between these two limits: it utilizes classical trajectories as 'input', and thus contains classical dynamics, and incorporates quantum mechanics approximately, i.e., within the SC approximation. The SC approximation actually contains *all* quantum effects at least qualitatively, and in molecular systems the description is usually quite quantitative. This was first demonstrated by work in the 1970's on small molecular systems (primarily scattering problems)[1-6], and more recently in applications to systems with many degrees of freedom by using various initial value representations (IVRs) of SC theory (primarily to calculate time correlation functions)[7-18].

The SC-IVR approach is also intermediate between classical MD and a full quantum treatment with regard to ease of application, i.e., it is more difficult to apply than standard classical

mechanics, but much easier (for large molecular systems) than a full quantum calculation. Within the SC-IVR framework, too, there is a 'sub-menu' of approaches, from the full SC-IVR treatment which entails no additional approximations, to other versions that introduce approximations beyond the SC approximation itself to make it easier to apply to complex systems.

The simplest (and most approximate) version of the SC-IVR is its 'linearized' approximation (LSC-IVR)[19-24], which leads to the classical Wigner model[25-27] for time correlation functions; see Section IIA for a summary of the LSC-IVR. The classical Wigner model is an old idea, but it is important to realize that it is contained within the SC-IVR approach, as a well-defined approximation to it. There are other ways to derive the classical Wigner model (or one may simply postulate it)[28-31], and we also note that the 'forward-backward semiclassical dynamics' (FBSD) approximation of Makri *et al*[32-39] is very similar to it. The LSC-IVR/classical Wigner model cannot describe true quantum coherence effects in time correlation functions—more accurate SC-IVR approaches, such as the Fourier transform forward-backward IVR (FB-IVR) approach[40,41] (or the still more accurate *generalized* FB-IVR[42]) of Miller *et al*, are needed for this—but it does describe a number of aspects of the dynamics very well[21-24,43]. E.g., the LSC-IVR has been shown to describe reactive flux correlation functions (which determine chemical reaction rates) quite well, including strong tunneling regimes[22], and velocity correlation functions in systems with enough degrees of freedom for quantum re-phasing to be unimportant[23,43].

Within the LSC-IVR approximation for thermal time correlation functions the most

challenging aspect of the calculation (beyond what is required for a purely classical MD calculation) is construction of the Wigner function involving the Boltzmann operator[23]. In a previous paper[23] the two of us showed that the thermal Gaussian approximation (TGA)[44-46] of Frantsuzov and Mandelshtam could be very fruitfully adapted for this purpose; Section IIB summarizes this approximation. Test calculations in our previous paper[23] showed that the TGA introduced no significant approximation beyond that of the LSC-IVR itself (at least for the applications considered). We have demonstrated that the combined TGA/LSC-IVR can be readily applied to condensed phase systems with a simulation of the dynamics of liquid neon near its triple point (around 29.90 K).

The purpose of this paper is to apply this combined TGA/LSC-IVR approach to two much more challenging examples, (a) a Ne_{13} Lennard-Jones (LJ) cluster in the temperature range $4\,\mathrm{K} \le T \le 14\,\mathrm{K}$, which encompasses the transition of the cluster from solid-like to liquid-like behavior, and (b) liquid *para*-hydrogen at two temperatures, 25 K and 14 K (under nearly zero external pressure). The Ne_{13} LJ cluster is such a demanding system that even its thermodynamic properties were not treated accurately until recently[45,47], since the simulation of quantum canonical ensemble of small neon clusters is far from trivial[48]. The present TGA/LSC-IVR simulation is the first study of quantum dynamical effects in this system. In the second example, liquid *para*-hydrogen, collective coherent excitations have been discovered[49,50], and its transport properties (e.g. self-diffusion constants) have been measured[51] and also studied by others with a variety of theoretical methods[43,52-56]. It thus serves as another useful benchmark system to test the applicability and accuracy of the

TGA/LSC-IVR approach.

Section II first summarizes the TGA/LSC-IVR methodology very briefly, and Section III then presents the results of the present applications. Section IV concludes.

II. METHODOLOGY

In this section we briefly review the TGA/LSC-IVR methodology[23] that we have developed recently. Our focus is on equilibrium time correlation functions[57] of systems at finite temperature, which are of the form

$$C_{AB}(t) = \mathrm{Tr}\left(\hat{A}^{\beta} e^{i\hat{H}t/\hbar} \hat{B} e^{-i\hat{H}t/\hbar}\right) \tag{2.1}$$

where $\hat{A}^{\beta} = \frac{1}{Z} e^{-\beta\hat{H}} \hat{A}$ for the standard version of the correlation function, or $\hat{A}^{\beta}_{sym} = \frac{1}{Z} e^{-\beta\hat{H}/2} \hat{A} e^{-\beta\hat{H}/2}$ for the symmetrized version[58], or $\hat{A}^{\beta}_{Kubo} = \frac{1}{Z\beta}\int_0^{\beta} \mathrm{d}\lambda e^{-(\beta-\lambda)\hat{H}} \hat{A} e^{-\lambda\hat{H}}$ for the Kubo-transformed version[59]. These three versions are related to one another by the following identities between their Fourier transforms,

$$\frac{\beta\hbar\omega}{1-e^{-\beta\hbar\omega}} \tilde{C}^{Kubo}_{AB}(\omega) = \tilde{C}_{AB}(\omega) = e^{\beta\hbar\omega/2} \tilde{C}^{sym}_{AB}(\omega) \tag{2.2}$$

where $\tilde{C}_{AB}(\omega) = \int_{-\infty}^{\infty} dt\, e^{-i\omega t} C_{AB}(t)$ etc. Here $\hat{H}$ is the (time-independent) Hamiltonian for the system, which for large molecular systems is usually expressed in terms of its Cartesian coordinates and momenta

$$\hat{H} = \tfrac{1}{2}\hat{\mathbf{p}}^{\mathrm{T}} \mathbf{M}^{-1} \hat{\mathbf{p}} + V\left(\hat{\mathbf{q}}\right) = \hat{H}_0 + V\left(\hat{\mathbf{q}}\right) \tag{2.3}$$

where $\mathbf{M}$ is the (diagonal) mass matrix and $\hat{\mathbf{p}}$, $\hat{\mathbf{q}}$ are the momentum and coordinate operators, respectively. Also, in Eq. (2.1) $Z = \mathrm{Tr} e^{-\beta \hat{H}}$ $\left(\beta = 1/k_B T\right)$ is the partition function, and $\hat{A}$ and $\hat{B}$ are operators relevant to the specific property of interest.

A. Linearized Semiclassical Initial Value Representation

The SC-IVR approximates the forward (backward) time evolution operator $e^{-i\hat{H}t/\hbar}$ ($e^{i\hat{H}t/\hbar}$) by a phase space average over the initial conditions of forward (backward) classical trajectories[1,7-9]. By making the (drastic but reasonable) approximation that the dominant contribution to the phase space averages comes from forward and backward trajectories that are close to one another and then linearizing the forward and backward actions of such trajectories, Miller and coworkers[19-21] obtained the linearized SC-IVR (LSC-IVR), or classical Wigner model for the correlation function

$$C_{AB}^{LSC-IVR}(t) = \int d\mathbf{x}_0 \int d\mathbf{p}_0 A_w^{\beta}(\mathbf{x}_0, \mathbf{p}_0) B_w(\mathbf{x}_t, \mathbf{p}_t) \tag{2.4}$$

where A_w^{β} and B_w are the Wigner functions[25] corresponding to these operators,

$$O_w(\mathbf{x}, \mathbf{p}) = \int d\boldsymbol{\Delta x} \left\langle \mathbf{x} - \boldsymbol{\Delta x}/2 \middle| \hat{O} \middle| \mathbf{x} + \boldsymbol{\Delta x}/2 \right\rangle e^{i\mathbf{p}^T \boldsymbol{\Delta x}/\hbar} \tag{2.5}$$

for any operator $\hat{O}$. Here $(\mathbf{x}_0, \mathbf{p}_0)$ is the set of initial conditions (i.e., coordinates and momenta) for a classical trajectory, $(\mathbf{x}_t(\mathbf{x}_0, \mathbf{p}_0), \mathbf{p}_t(\mathbf{x}_0, \mathbf{p}_0))$ being the phase point at time t along that trajectory. The LSC-IVR approximation for the time correlation function approaches the classical limit at high temperature, and for the case of a harmonic potential it gives the exact quantum correlation function for all time t and for arbitrary operators $\hat{A}$ and $\hat{B}$; it also gives the correct quantum result as $t \to 0$ for arbitrary potentials. The LSC-IVR can be applied not only to

correlation functions at equilibrium but also to non-equilibrium correlation functions. These merits of the LSC-IVR make it a versatile tool to study quantum-mechanical effects in chemical dynamics of complex (large) systems.

The LSC-IVR formulation of the time correlation function has also been obtained from a different approach by Pollak and Liao[28], Shi and Geva[29], and Rossky *et al*[30] by adopting a similar linearization approximation but to the real time path integral representation of the time evolution operators in the correlation function. More recently, Liu and Miller[31] have shown that the *exact* quantum time correlation function can be expressed in the same form as Eq. (2.4), with an associated dynamics in the single phase space, and it was furthermore demonstrated that the LSC-IVR is its classical limit $\hbar \to 0$, high temperature limit $\beta \to 0$, and harmonic limit. This formulation thus suggests ways to improve the LSC-IVR without having to deal with the phase cancellation problems in the full version of the SC-IVR.

Calculation of the Wigner function for operator $\hat{B}$ in Eq. (2.4) is usually straight-forward; in fact, $\hat{B}$ is often a function only of coordinates or only of momenta, in which case its Wigner function is simply the classical function itself. Calculating the Wigner function $A_w^\beta(\mathbf{x}_0, \mathbf{p}_0)$, however, involves the Boltzmann operator with the total Hamiltonian of the complete system, so that carrying out the multidimensional Fourier transform to obtain it is far from trivial. Furthermore, it is necessary to do this in order to obtain the distribution of initial conditions of momenta $\mathbf{p}_0$ for the real time trajectories. A rigorous way to treat the Boltzman operator is via a Feynman path integral

expansion, but it is then in general not possible to evaluate the multidimensional Fourier transform explicitly to obtain the Wigner function $A_w^\beta(\mathbf{x}_0, \mathbf{p}_0)$, as discussed by Liu and Miller[23]. The inability to calculate the Wigner function of $\hat{A}^\beta$ exactly is in fact the reason for the various harmonic and local harmonic approximations to the Boltzmann operator[20,23,24,30] that have been used in implementing the LSC-IVR. These approximations have been successfully applied to several interesting complex systems[23,43,60].

B. LSC-IVR Correlation Functions Using the Thermal Gaussian Approximation

Here we use the thermal Gaussian approximation[44-46] (TGA) of Frantsuzov and Mandelshtam to construct the Boltzmann operator as necessary for the LSC-IVR[16]. In the TGA, the Boltzmann matrix element is approximated by a Gaussian form:

$$\langle \mathbf{x} | e^{-\tau \hat{H}} | \mathbf{q_0} \rangle = \left(\frac{1}{2\pi} \right)^{3N/2} \frac{1}{\left| \det(\mathbf{G}(\tau)) \right|^{1/2}} \exp\left(-\frac{1}{2} (\mathbf{x} - \mathbf{q}(\tau))^T \mathbf{G}^{-1}(\tau) (\mathbf{x} - \mathbf{q}(\tau)) + \gamma(\tau) \right) \qquad (2.6)$$

where $\mathbf{G}(\tau)$ is an imaginary-time dependent real symmetric and positive-definite matrix, $\mathbf{q}(\tau)$ the center of the Gaussian, and $\gamma(\tau)$ a real scalar function. The parameters are governed by the equations of motion in imaginary time which were given explicitly in our previous paper[23] and in other references[44-46]. The matrix $\mathbf{G}(\tau)$ is a full $3N \times 3N$ matrix, where N is number of particles of the system. To simplify the calculation further, in reference[45] Frantsuzov and Mandelshtam approximated the matrix $\mathbf{G}(\tau)$ by neglecting off-diagonal elements between different particles, so that it becomes a block diagonal matrix with N blocks of 3×3 real symmetric matrices, one for each particle. We term the former (with the full **G** matrix) as the 'Full-TGA', and

the latter (with the single particle approximation) as the 'SP-TGA'. Recent applications have shown the TGA to be a good approximation for the thermodynamic properties of some complex systems (neon clusters) even at very low temperature[45,61,62].

The TGA for the Boltzmann operator makes it possible to perform the Fourier transform necessary to construct the Wigner function of operator $\hat{A}^{\beta}$ analytically; specifically, $A_w^{\beta}\left(\mathbf{x}_0,\mathbf{p}_0\right)$ in Eq. (2.4) is given as follows[23]

$$\begin{aligned} A_w^{\beta}\left(\mathbf{x}_0,\mathbf{p}_0\right) = & \frac{1}{Z}\int d\mathbf{q}_0 \frac{1}{\left(4\pi\right)^{3N/2}} \frac{\exp\left(2\gamma\left(\frac{\beta}{2}\right)\right)}{\left|\det \mathbf{G}\left(\frac{\beta}{2}\right)\right|^{1/2}} \\ & \cdot \frac{1}{\pi^{3N/2}\left|\det \mathbf{G}\left(\frac{\beta}{2}\right)\right|^{1/2}} \exp\left(-\left(\mathbf{x}_0-\mathbf{q}\left(\frac{\beta}{2}\right)\right)^T \mathbf{G}^{-1}\left(\frac{\beta}{2}\right)\left(\mathbf{x}_0-\mathbf{q}\left(\frac{\beta}{2}\right)\right)\right) \\ & \cdot \frac{\left|\det \mathbf{G}\left(\frac{\beta}{2}\right)\right|^{1/2}}{\left(\pi\hbar^2\right)^{3N/2}} \exp\left(-\mathbf{p}_0^T \mathbf{G}\left(\frac{\beta}{2}\right)\mathbf{p}_0/\hbar^2\right) \\ & \cdot f_{A^{\beta}}^{TGA}\left(\mathbf{x}_0,\mathbf{p}_0,\mathbf{q}\left(\frac{\beta}{2}\right)\right) \end{aligned} \tag{2.7}$$

where for two Kubo-transformed time correlation functions studied in this paper

$$f_{A^{\beta},\,Kubo}^{TGA-LSC-IVR}\left(\mathbf{x}_0,\mathbf{p}_0,\mathbf{q}\left(\tfrac{\beta}{2}\right)\right) = -\tfrac{2}{\beta}\mathbf{G}^{-1}\left(\tfrac{\beta}{2}\right)\left(\mathbf{x}_0-\mathbf{q}\left(\tfrac{\beta}{2}\right)\right) \tag{2.8}$$

for the force operator $\hat{A}=\mathbf{f}\left(\hat{\mathbf{x}}\right)=-V'\left(\hat{\mathbf{x}}\right)$ with $\hat{A}_{Kubo}^{\beta}=\frac{1}{\beta}\int_0^{\beta} d\lambda e^{-(\beta-\lambda)\hat{H}}\mathbf{f}\left(\hat{\mathbf{x}}\right)e^{-\lambda\hat{H}}$, and

$$f_{A^{\beta},\,Kubo}^{TGA-LSC-IVR}\left(\mathbf{x}_0,\mathbf{p}_0,\mathbf{q}\left(\tfrac{\beta}{2}\right);t\right) = \tfrac{2}{\hbar^2\beta}\mathbf{MG}\left(\tfrac{\beta}{2}\right)\mathbf{p}_0 \tag{2.9}$$

for the momentum operator $\hat{A}=\hat{\mathbf{p}}$ with $\hat{A}_{Kubo}^{\beta}=\frac{1}{\beta}\int_0^{\beta} d\lambda e^{-(\beta-\lambda)\hat{H}}\hat{\mathbf{p}}e^{-\lambda\hat{H}}$.

Monte Carlo (MC) evaluation of Eq. (2.4) together with Eq. (2.7) is now straightforward, and we refer readers to Section IV of our recent paper[23] for more details.

Compared with the Feynman-Kleinert (FK) approximation used by Poulsen *et al*[30] and the local harmonic approximation (LHA) of by Shi and Geva[24], the TGA avoids the imaginary frequency

problem inherent in the former two approximations[24,30,43,60]. Furthermore, the computational cost of the Full-TGA is dominated by the Cholesky factorization of a $3N \times 3N$ matrix while that of the FK approximation and the LHA is dominated by the diagonalization of such a matrix. Also, in many cases the SP-TGA approximates the Full-TGA sufficiently well (as shown in next section), and this decreases the computational effort even further by having to deal only with the factorization of a block diagonal matrix (of N 3×3 blocks, each of which represents a single particle).

In our previous paper the TGA/LSC-IVR was successfully applied to a one-dimensional anharmonic model and to liquid neon near its triple point[23]. In next section, we use it to study two more challenging condensed phase systems.

III. APPLICATIONS

A. Ne_{13} Lennard-Jones cluster

Clusters, i.e., aggregates of atoms or molecules ranging from several monomer units up to nano-particles, which bridge the gap between our understanding of molecules and that of the bulk, have attracted much attentions in both experimental and theoretical research over the last decade[48,63-68]. Due to their finite size, structural and dynamical properties of clusters are usually distinct from those of bulk matter[48,67-71]. Phase transitions have also been an active research topic of clusters for many years[48,67,68]. Since a true phase transition can only occur in systems in the thermodynamic limit ($N \to \infty, V \to \infty,$ and $N/V = \text{constant}$, where N is number of particles of the system and V is its volume)[72,73], the behavior of such phenomena is clusters is different from that in bulk matter[48,67-71];

e.g., the melting transition shows an abrupt discontinuity in characteristic thermodynamic functions at the melting temperature, while in finite-sized clusters this behavior is smoothed out, with a remnant of such behavior persisting over a finite range of temperature[67].

Because of the finite size of a small cluster, the temperature at constant energy may fluctuate dramatically. Canonical simulations assume a statistical ensemble of non-interacting clusters in thermal contact with a macroscopic heat bath which defines the temperature of the cluster[48]. The canonical ensemble has proved to be very useful to shed light on our detailed understanding of clusters[48,67,68]. Quantum canonical simulations of small clusters tend to be a much more difficult task than those of bulk counterparts. Although both a classical thermodynamic description of the Ar_{13} LJ cluster (where quantum effects are negligible) and a quantum canonical simulation of liquid bulk neon were available about twenty years ago[67,74], it was not until several years ago that the quantum thermodynamic properties of the Ne_{13} LJ cluster were accurately calculated by the path integral Monte Carlo (PIMC)[47] and by the TGA[45]. The recent developed TGA/LSC-IVR method[23] now enables us to simulate quantum dynamical effects in the Ne_{13} LJ cluster at thermal equilibrium for the first time.

We use the same potential energy function as in previous work[45,47]: the LJ parameters are $\varepsilon = 35.6\,\mathrm{K}$ and $\sigma = 2.749\,\mathring{\mathrm{A}}$; the mass of Ne atom is taken to be $m = 3.35\times10^{-26}$ kg. A confining constraint restricts the initial positions of the Gaussians used in the TGA to a spherical region which satisfies $\left|\mathbf{q}_i - \mathbf{R}_c\right| \le 2\sigma$, where $\mathbf{q}_i$ is the initial position of *i*-th neon atom in the initial Gaussian and $\mathbf{R}_c$ is the position of the center of mass of the cluster. The authors of the reference[47] discussed the

necessity for applying the confining constraint and why the results are insensitive to the radius of the confining sphere so long as it is large enough. To accelerate the imaginary time propagation in the TGA, we use the same fitting parameters as in the reference[45], i.e., the LJ potential is fit by a linear combination of Gaussians:

$$4\varepsilon\left[\left(\frac{\sigma}{r_{ij}}\right)^{12}-\left(\frac{\sigma}{r_{ij}}\right)^{6}\right]\approx\varepsilon\sum_{p=1}^{3}c_p\exp\left[-\alpha_p\sigma^{-2}r_{ij}^2\right] \tag{3.1}$$

with $\left\{\left(c_p,\alpha_p\right)\right\}=\left\{(1840,6.65),(-1.48,0.79),(-23.2,2.6)\right\}$ such that Gaussian integrals can be evaluated analytically.

The temperature range that we study is $4\,\mathrm{K}\le T\le 14\,\mathrm{K}$, which includes the melting transition (around $6\,\mathrm{K}-12\,\mathrm{K}$). As in reference[45], the standard metropolis algorithm is used for the imaginary time propagation of Gaussians in the TGA. Each initial Gaussian is selected by randomly shifting one of the particles so that the acceptance ratio of this random move is about 40%. The initial inverse temperature of the Gaussians is 0.0001β and they are propagated until imaginary time $\beta/2$. The imaginary time step is $d\beta=1/1456\left(k_B\,\mathrm{K}\right)^{-1}$, i.e., about 180 time steps are used for the temperature $T=4\,\mathrm{K}$. We first use 5.2×10^4 imaginary trajectories to equilibrate the system, then 2.08×10^5 imaginary trajectories with the Full-TGA are propagated to estimate thermodynamic properties. When time correlation functions are to be calculated, 10 real time trajectories, according to the initial phase points generated by each imaginary trajectory, are propagated with the usual velocity Verlet algorithm with a time step of $0.5\,\mathrm{fs}$.

The average energy per particle of the Ne_{13} LJ cluster system is shown in Fig. 1 for the entire

temperature range $4\,\mathrm{K} \le T \le 14\,\mathrm{K}$ for three different methods: the PIMC, the Full-TGA and the classical Monte Carlo (CMC). The most recent PIMC result is provided by Predescu[75] . Fig. 1 shows that the Full-TGA results agree well with the PIMC results and that the remnant of the liquid-solid phase transition occurs in that temperature range for both the quantum system and the classical system, which is consistent with the results in reference[45]. Comparison of the PIMC and Full-TGA results to the CMC results clearly reveals significant quantum statistical effects in the Ne_{13} LJ cluster.

The TGA/LSC-IVR, however, enables one to study quantum *dynamical* behavior of the Ne_{13} LJ cluster in the temperature region of the melting transition for the first time. Three temperatures are chosen: (a) $T = 14\,\mathrm{K}$ in the liquid-like region; (b) $T = 8\,\mathrm{K}$ in the middle of the melting phase transition region; and (c) $T = 4\,\mathrm{K}$ in the solid-like region. Fig. 2 shows the Kubo-transformed force autocorrelation function per particle, which reflects vibrations between particles and the structural information of the cluster. The Kubo-transformed force autocorrelation function is calculated by Eq. (2.4) together with Eqs. (2.7) and (2.8). The TGA/LSC-IVR and classical results are qualitatively similar in the liquid-like region (panel a), but show significant differences in the transition region (panel b) and the solid-like region (panel c). Though the TGA/LSC-IVR correlation function shows some structure at longer time (past the minimum), it is much reduced from that given by the classical calculation, indicating that particles in the Ne_{13} LJ cluster in the solid-like region are much more mobile in the semiclassical treatment than in the classical case, due to

significant quantum dynamical effects.

The major conclusion from these calculations, therefore, is that the phase transitional behavior in the Ne_{13} cluster shows up in *thermodynamic* properties to a very similar degree in classical and semiclassical treatments (cf. Fig. 1), with some quantitative differences, while the semiclassical description of *dynamica*l properties (e.g., the force-force correlation functions in Fig. 2) shows significant qualitative differences from the classical treatment. I.e., quantum effects in dynamical properties seem to be more significant than those in thermodynamic properties (apart from an energy scaling).

B. Liquid *para*-hydrogen

Though H_2 is the lightest and thus most quantum-like molecule, quantum effects due to exchange of identical molecules are negligible in its liquid phase. This is because the temperature of liquid hydrogen is so high (above 13.8 K) that the de Broglie thermal wavelength $\lambda = h/\left(2\pi m k_B T\right)^{1/2}$ is not large enough to overlap the region of the normal distance between two interacting molecules (unlike the situation with liquid helium at ~ 2 K). This greatly simplifies the treatment since the dynamical description of quantum exchange is not a trivial task.

Liquid *para*-hydrogen is well described by the Silvera-Goldman (SG) model[76], an isotropic pair potential in which the *para*-hydrogen molecule is treated as a sphere particle. (The spherical approximation is known to be accurate because the temperature of liquid *para*-hydrogen is much too low for any rotational state other than J = 0 to be populated.) The SG potential takes the form

$$V(r) = \exp(\alpha - \beta r - \gamma r^2) - \left(\frac{C_6}{r^6} + \frac{C_8}{r^8} + \frac{C_{10}}{r^{10}}\right) f_c(r) + \frac{C_9}{r^9} f_c(r) \tag{3.2}$$

where

$$f_c(r) = \begin{cases} \exp\left[-(r_c / r - 1)^2\right] & (r \le r_c) \\ 1 & (r > r_c) \end{cases} \tag{3.3}$$

with the parameters listed in Table 1. The first term on the right-hand side of Eq. (3.2) represents the exponential SCF short-range repulsive interaction, the second one is the asymptotic long-range van der Waals attractive interaction, attenuated by $f_c(r)$ at short distances, and the third one is an effective two-body approximation to the three-body Axilrod-Teller-Muto triple-dipole dispersion interaction[76]. The SG potential has been widely used to study thermodynamic properties and been shown to give reasonable agreement with experimental data[77].

A variety of theoretical approaches have been used to calculate the self-diffusion constant of liquid *para*-hydrogen, e.g., maximum entropy (numerical) analytic continuation (MEAC)[53], quantum mode-coupling theory (QMCT)[52], centroid molecular dynamics (CMD)[56,78,79], ring-polymer molecular dynamics (RPMD)[55,56], forward-backward semiclasical dynamics (FBSD)[54], and Feynman-Kleinert linearized path integral (FK-LPI)[43]. The FK-LPI is in fact the LSC-IVR using the FK approximation for the Boltzmann operator. Here we revisit the simulation of the self-diffusion constant of liquid *para*-hydrogen using the TGA/LSC-IVR and compare the results with experimental measurements and other theoretical predictions.

Our simulations (using periodic boundary conditions with 108 molecules per cell with the

minimum image convention) focus on two thermodynamic state points (25 K with molar volume $\upsilon = 31.7\,\mathrm{cm^3 mol^{-1}}$ and 14 K with molar volume $\upsilon = 25.6\,\mathrm{cm^3 mol^{-1}}$) which were obtained from previous PIMC calculations under nearly zero external pressure[77]. To accelerate the imaginary time propagation in the TGA, we use the same fit of the SG potential to a linear combination of Gaussians as in reference[43],

$$V(r) \approx \sum_{p=1}^{4} c_p \exp\left[-\alpha_p r_{ij}^2\right] \tag{3.4}$$

with

$$\begin{aligned}\left\{\left(c_p, \alpha_p\right)\right\} = \Big\{&\left(0.30580, 0.29074\right), \left(-6.1893\times10^{-5}, 0.018674\right), \\ &\left(0.046165, 0.16729\right), \left(-1.1568\times10^{-3}, 0.055019\right)\Big\}\end{aligned} \tag{3.5}$$

in atomic units. As in the previous application in Section IIIA, the standard metropolis algorithm is implemented and the acceptance ratio of new initial Gaussians is about 40%. The initial inverse temperature of starting Gaussians is 0.0001β. About 5×10^4 imaginary trajectories are used for initial equilibrations, then during the simulation of the correlation function, the total number of imaginary trajectories is 2×10^6 and the imaginary time step at the state point 25 K is 15 while that at 14 K is 20. Both the Full-TGA and the SP-TGA are implemented. Our calculation involves the Kubo-transformed momentum autocorrelation function (i.e., Eq. (2.4) together with Eqs. (2.7) and (2.9)), and it is easy to verify that the TGA/LSC-IVR formulation of the Kubo-transformed momentum autocorrelation function gives the exact quantum mechanical result obtained from Eq. (2.1) as $t \to 0$, i.e.,

$$\lim_{t\to 0} C_{\mathbf{pp},\,Kubo}^{TGA-LSC-IVR}(t) = \frac{3m}{\beta} \tag{3.6}$$

Only one real time trajectory with the use of the velocity Verlet algorithm with a time step of $0.5\,\mathrm{fs}$ per imaginary time trajectory is sufficient to provide converged results.

Fig. 3 shows our results for the Kubo-transformed momentum autocorrelation functions per molecule (divided by $2mk_B$) performed by the LSC-IVR with the Full-TGA and with the SP-TGA. The error bars of the results are smaller than the widths of the plotted curves. For comparison, Fig. 3 also shows results of the RPMD[55] and those of the recent improved version of the RPMD which combines it with the MEAC (RPMD+MEAC), as proposed by Manolopoulos and coworkers[80]. Panel (a) shows the results for the autocorrelation function at $T = 25\,\mathrm{K}$. The Full-TGA and the SP-TGA are seen to be essentially identical, exhibiting a smooth and monotonic decay to zero at long time. They agree well with the work of Poulsen *et al* (Figure 5 in reference[43]), which is expected since the latter is also an implementation of the LSC-IVR. The results of the RPMD[55] and CMD[79] (not shown, but similar) decay to zero significantly faster than the LSC-IVR results, while the RPMD+MEAC agrees with the TGA/LSC-IVR much better, deviating only slightly at long time.

Panel (b) shows the results for the lower temperature, $T = 14\,\mathrm{K}$. The SP-TGA still provides a good approximation to the Full-TGA. The autocorrelation function decays much faster in this case and has a minimum at ~ 0.25 ps, indicating that impulsive, velocity-reversing collisions appear in this lower temperature and high density regime. The RPMD[55] and CMD[79] (not shown) correlation functions show similar behavior but have a deeper minimum. The RPMD+MEAC result again

agrees with the TGA/LSC-IVR result much better at short times and has a minimum that is intermediate between that of the RPMD and the LSC-IVR, though both the RPMD+MEAC and the RPMD results decay to zero much more slowly than the LSC-IVR.

For both temperatures, the qualitative differences at longer times between these methods affect their prediction of the diffusion constant (see below) and simply demonstrate that the true behavior of the quantum correlation function at long time is still an open issue. However, the good agreement between the TGA/LSC-IVR and the RPMD+MEAC at short times ($\lesssim \hbar\beta$) is encouraging and suggests they are giving the correct result in this regime.

The Fourier transform relations in Eq. (2.2) enable one to express the average kinetic energy $\left\langle \hat{\mathbf{p}}^2/2m \right\rangle$ in terms of the Kubo-transformed momentum autocorrelation function. It is straightforward to show

$$\left\langle \frac{\hat{\mathbf{p}}^2}{2m} \right\rangle = \frac{1}{4\pi m} \int_{-\infty}^{\infty} d\omega \frac{\beta\hbar\omega}{\left(1-e^{-\beta\hbar\omega}\right)} \int_{-\infty}^{\infty} dt\, e^{-i\omega t} C_{\mathbf{pp}}^{kubo}(t) \tag{3.7}$$

In literature[43,55], Eq. (3.7) has been used to test the behavior of the Kubo-transformed momentum autocorrelation function. Recently Braams *et al*[81] have shown that this test is only sensitive to the values of the Kubo-transformed correlation function for times on the order of $\hbar\beta$. Table 2 lists the TGA/LSC-IVR Kubo-based average kinetic energies together with the PIMC results. The TGA/LSC-IVR Kubo-based average kinetic energies deviate from the PIMC results by no more than 4%. The SP-TGA agrees well with the Full-TGA at 25 K and shows only a small difference at 14 K, verifying that the SP-TGA is an adequate approximation for the Kubo-transformed momentum

autocorrelation function. In Table 2, the TGA/LSC-IVR results are directly compared with the FK-LPI result[43] for $T = 25\,\mathrm{K}$ and the RPMD results[55] for both state points, demonstrating that the TGA/LSC-IVR Kubo-transformed correlation function satisfies Eq. (3.7) quite well.

Recent work by Nakayama and Makri[82] provides another more interesting way to test the behavior of the Kubo-transformed momentum autocorrelation function. They have used the pair-product approximation to the complex time quantum mechanical propagator and computed accurate PIMC results for the first 0.2 ps of the symmetrized momentum autocorrelation function of liquid *para*-hydrogen at the state point, $T = 25\,\mathrm{K}, \upsilon = 31.7\,\mathrm{cm^3 mol^{-1}}$; these should very likely be the definitive quantum results for this system in this short time regime. Using the Fourier transform relations in Eq. (2.2), the symmetrized autocorrelation function can be expressed in terms of the Kubo-transformed autocorrelation function , i.e.,

$$C_{\mathbf{pp}}^{sym}(t) = \frac{1}{2\pi}\int_{-\infty}^{\infty} d\omega\, e^{i\omega t}\,\frac{\beta\hbar\omega/2}{\sinh(\beta\hbar\omega/2)}\int_{-\infty}^{\infty} dt'\, e^{-i\omega t'} C_{\mathbf{pp}}^{kubo}(t') = \frac{\pi}{2\beta\hbar}\int_{-\infty}^{\infty} dt' \mathrm{sech}^2\left[\frac{\pi(t-t')}{\beta\hbar}\right] C_{\mathbf{pp}}^{kubo}(t') \quad , \tag{3.8}$$

so that it is possible to convert all of the above Kubo-transformed correlation functions in Fig. 3 into their symmetrized versions and thus be able to compare them to these accurate complex time PIMC results of Nakayama and Makri[80,82]. Fig. 4 shows these comparisons at $T = 25\,\mathrm{K}$. One sees that the TGA/LSC-IVR, MEAC, and RPMD+MEAC results are all in very good agreement with the accurate PIMC correlation function for this short time period ($\lesssim$ 0.2 ps), with the FBSD result only slightly further off and the RPMD somewhat more so. Unfortunately, the complex time PIMC

results of Nakayama and Makri are not reliable beyond ~0.2 ps[82] for $T = 25\,\mathrm{K}$, and accurate PIMC results are not available at present for the $T = 14\,\mathrm{K}$ state point. Thus further work is needed to obtain accurate benchmark results for longer time and lower temperature.

The self-diffusion coefficient is given in terms of the time integral of the momentum autocorrelation function (for any of those in Eq. (2.1)),

$$D = \frac{1}{3m^2 N}\int_0^\infty C_{\mathbf{pp}}(t)\,dt \quad . \tag{3.9}$$

Table 3 gives the LSC-IVR (with the Full-TGA and with the SP-TGA) results so obtained for the diffusion coefficient at the two state points $T = 25\,\mathrm{K}, \upsilon = 31.7\,\mathrm{cm^3 mol^{-1}}$ and $T = 14\,\mathrm{K}, \upsilon = 25.6\,\mathrm{cm^3 mol^{-1}}$ under nearly zero extent pressure, together with other theoretical and experimental results. The various theoretical results show reasonable agreement with experimental values, with all of the approximate quantum results being in better agreement with each other than with the classical values. Again, the SP-TGA is seen to be a good approximation to the Full-TGA.

Among trajectory-based methods, we note that the two simplest semiclassical methods (the LSC-IVR and the FBSD) overestimate the self-diffusion constants slightly at 25 K and by over 50% at 14 K, while the CMD and the RPMD underestimate the results at these two state points. The differences come mainly from the long time behavior of the correlation functions. As pointed out by Manolopoulos *et al.*, however, one should not read too much into the comparison with experiment[80], for there is some error in the use the SG potential, to which the dynamical behavior at long times is sensitive; e.g., the fact that the thermodynamic properties (e.g., molar volumes) obtained from the

PIMC simulations with the SG potential do not show precise agreement with experiments at either temperature[77] is indicative that the potential is not highly accurate.

IV. CONCLUSIONS

In this paper we have applied the TGA/LSC-IVR approach to study quantum dynamical effects in realistic models of two condensed phase systems: the Ne_{13} LJ cluster, the first such treatment of its quantum dynamics, and liquid *para*-hydrogen, which has been treated by a number of theoretical approaches and thus makes an excellent benchmark system. Since quantum thermodynamic properties calculated for the Ne_{13} cluster by the PIMC and the TGA show liquid-solid phase transitional structure between 4 K and 14 K, this was the temperature region we investigated. The Kubo-transformed force autocorrelation functions calculated by the TGA/LSC-IVR in that region, however, show little of the solid-like structure that is seen in the classical correlation function; i.e., due to quantum dynamical effects, the TGA/LSC-IVR correlation function is much more liquid-like, indicating that the atoms are much more mobile quantum mechanically than they are classically. Liquid-solid phase transitional behavior in the Ne_{13} LJ cluster is thus not as evident in its dynamical properties as it is thermodynamically.

Liquid *para*-hydrogen was also studied at two state points, $T = 25\,\mathrm{K}, \upsilon = 31.7\,\mathrm{cm^3 mol^{-1}}$ and $T = 14\,\mathrm{K}; \upsilon = 25.6\,\mathrm{cm^3 mol^{-1}}$, under nearly zero extent pressure. The Kubo-transformed momentum autocorrelation functions were calculated by the LSC-IVR, both with the Full-TGA and with the simpler SP-TGA, and it was seen that the SP-TGA is a very good approximation to the Full-TGA also

in this case. The kinetic energy obtained from the Kubo-transformed correlation function at each temperature agrees quite well with the PIMC result (no more than 4% error). The symmetrized momentum autocorrelation function at $25\,K$ agrees essentially perfectly with the accurate PIMC results over the initial time period ($\lesssim 0.2$ ps) for which it is available, and the self-diffusion constants calculated from the TGA/LSC-IVR method show reasonably good agreements with experimental values and other theoretical results.

The TGA/LSC-IVR thus provides a practical and versatile method for studying dynamical processes semi-quantitatively in condensed phase systems where quantum mechanics play a significant role. It will be interesting in future work to apply the TGA/LSC-IVR to study other problems, such as vibrational energy relaxation in molecular liquids, which involves correlation functions of highly nonlinear operators for which the LSC-IVR is still a good approximation[24,60,83-85].

ACKNOWLEDGEMENT

This work was supported by the Office of Naval Research Grant No. N00014-05-1-0457 and by the Director, Office of Science, Office of Basic Energy Sciences, Chemical Sciences, Geosciences, and Biosciences Division, U.S. Department of Energy under Contract No. DE-AC02-05CH11231. We also acknowledge a generous allocation of supercomputing time from the National Energy Research Scientific Computing Center (NERSC). J. L. gratefully thanks C. Predescu for stimulating discussions on the liquid Ne_{13} cluster and for his providing the most recent PIMC data of that system. We also thank D. Manolopoulos for providing the RPMD and the

RPMD+MEAC results on liquid *para*-hydrogen, and A. Nakayama and N. Makri for providing the FBSD and the complex time PIMC results on that system in reference[82].

References

[1] W. H. Miller, Adv. Chem. Phys. **25**, 69 (1974).

[2] W. H. Miller, Adv. Chem. Phys. **30**, 77 (1975).

[3] W. H. Miller, J. Chem. Phys. **53**, 3578 (1970).

[4] R. A. Marcus, J. Chem. Phys. **54**, 3965 (1971).

[5] R. A. Marcus, J. Chem. Phys. **56**, 3548 (1972).

[6] E. J. Heller, J. Chem. Phys. **62**, 1544 (1975).

[7] W. H. Miller, J. Phys. Chem. A **105** (13), 2942 (2001).

[8] W. H. Miller, Proc. Nat. Acad. Sci. USA. **102** (19), 6660 (2005).

[9] W. H. Miller, J. Chem. Phys. **125** (13), 132305 (2006).

[10] M. F. Herman and E. Kluk, Chem. Phys. **91**, 27 (1984).

[11] E. J. Heller, J. Chem. Phys. **95** (12), 9431 (1991).

[12] E. J. Heller, J. Chem. Phys. **94** (4), 2723 (1991).

[13] K. G. Kay, J. Chem. Phys. **100**, 4377 (1994).

[14] K. G. Kay, J. Chem. Phys. **100**, 4432 (1994).

[15] G. Campolieti and P. Brumer, Phys. Rev. A **50** (2), 997 (1994).

[16] J. Wilkie and P. Brumer, Phys. Rev. A **61**, 064101 (2001).

[17] M. Thoss and H. B. Wang, Ann. Rev. Phys. Chem. **55**, 299 (2004).

[18] K. G. Kay, Ann. Rev. Phys. Chem. **56**, 255 (2005).

[19] X. Sun and W. H. Miller, J. Chem. Phys. **106** (3), 916 (1997).

[20] H. Wang, X. Sun, and W. H. Miller, J. Chem. Phys. **108** (23), 9726 (1998).

[21] X. Sun, H. Wang, and W. H. Miller, J. Chem. Phys. **109** (17), 7064 (1998).

[22] T. Yamamoto and W. H. Miller, J. Chem. Phys. **118** (5), 2135 (2003).

[23] J. Liu and W. H. Miller, J. Chem. Phys. **125** (22), 224104 (2006).

[24] Q. Shi and E. Geva, J. Phys. Chem. A **107**, 9059 (2003).

[25] E. P. Wigner, Phys. Rev. **40**, 749 (1932).

[26] E. J. Heller, J. Chem. Phys. **65**, 1289 (1976).

[27] H. W. Lee and M. O. Scully, J. Chem. Phys. **73** (5), 2238 (1980).

[28] E. Pollak and J. L. Liao, J. Chem. Phys. **108** (7), 2733 (1998).

[29] Q. Shi and E. Geva, J. Chem. Phys. **118** (18), 8173 (2003).

[30] J. A. Poulsen, G. Nyman, and P. J. Rossky, J. Chem. Phys. **119**, 12179 (2003).

[31] J. Liu and W. H. Miller, J. Chem. Phys. **126**, 234110 (2007).

[32] J. Shao and N. Makri, J. Phys. Chem. A **103**, 7753 (1999).

[33] J. Shao and N. Makri, J. Phys. Chem. A **103**, 9479 (1999).

[34] N. Makri, J. Phys. Chem. B **106** (33), 8390 (2002).

[35] N. J. Wright and N. Makri, J. Phys. Chem. B **108**, 6816 (2004).

[36] A. Nakayama and N. Makri, Chem. Phys. **304**, 147 (2004).

[37] A. Nakayama and N. Makri, Proc. Nat. Acad Sci. USA **102**, 4230 (2005).

[38] J. Liu and N. Makri, Chem. Phys. **322** (1-2), 23 (2006).

[39] J. Liu, A. Nakayama, and N. Makri, Mol. Phys. **104** (8), 1267 (2006).

[40] W. H. Miller, Faraday Discuss. (110), 1 (1998).

[41] X. Sun and W. H. Miller, J. Chem. Phys. **110** (14), 6635 (1999).

[42] M. Thoss, H. Wang, and W. H. Miller, J. Chem. Phys. **114** (21), 9220 (2001).

[43] J. A. Poulsen, G. Nyman, and P. J. Rossky, J. Phys. Chem. B **108** (51), 19799 (2004).

[44] P. Frantsuzov, A. Neumaier, and V. A. Mandelshtam, Chem. Phys. Lett. **381** (1-2), 117 (2003).

[45] P. A. Frantsuzov and V. A. Mandelshtam, J. Chem. Phys. **121** (19), 9247 (2004).

[46] J. S. Shao and E. Pollak, J. Chem. Phys. **125** (13) (2006).

[47] C. Predescu, D. Sabo, J. D. Doll, and D. L. Freeman, J. Chem. Phys. **119** (23), 12119 (2003).

[48] D. L. Freeman and J. D. Doll, Annu. Rev. Phys. Chem. **47**, 43 (1996).

[49] F. J. Bermejo, B. Fak, S. M. Bennington, R. Fernandez-Perea, C. Cabrillo, J. Dawidowski, M. T. Fernandez-Diaz, and P. Verkerk, Phys. Rev. B **60** (22), 15154 (1999).

[50] F. J. Bermejo, K. Kinugawa, C. Cabrillo, S. M. Bennington, B. Fak, M. T. Fernandez-Diaz, P. Verkerk, J. Dawidowski, and R. Fernandez-Perea, Phys. Rev. Lett. **84** (23), 5359 (2000).

[51] B. N. Esel'son, Y. P. Blagoi, V. V. Grigor'ev, V. G. Manzhelii, S. A. Mikhailenko, and N. P. Neklyudov, *Properties of Liquid and Solid Hydrogen*. (Israel Program for Scientific Translations, Jerusalem, 1971).

[52] D. R. Reichman and E. Rabani, J. Chem. Phys. **116**, 6279 (2002).

[53] E. Rabani, D. R. Reichman, G. Krilov, and B. J. Berne, Proc. Nat. Acad Sci. USA **99**, 1129 (2002).

[54] A. Nakayama and N. Makri, J. Chem. Phys. **119**, 8592 (2003).

[55] T. F. Miller and D. E. Manolopoulos, J. Chem. Phys. **122** (18) (2005).

[56] T. D. Hone, P. J. Rossky, and G. A. Voth, J. Chem. Phys. **124** (15) (2006).

[57] B. J. Berne and G. D. Harp, Adv. Chem. Phys. **17**, 63 (1970).

[58] W. H. Miller, S. D. Schwartz, and J. W. Tromp, J. Chem. Phys. **79** (10), 4889 (1983).

[59] R. Kubo, M. Toda, and N. Hashitsume, *Statistical Physics*, 2nd ed. (Springer-Verlag, Heidelberg, 1991).

[60] Q. Shi and E. Geva, J. Phys. Chem. A **107** (9070-9078) (2003).

[61] P. A. Frantsuzov, D. Meluzzi, and V. A. Mandelshtam, Phys. Rev. Lett. **96** (11), 113401 (2006).

[62] P. A. Frantsuzov and V. A. Mandelshtam, Phys. Rev. E **72** (3), 37102 (2005).

[63] R. B. K. Jena P., Khanna S. N., *Physics and Chemistry of Small Clusters*. (Plenum, New York, 1987).

[64] O. Echt and E. Recknagel, Z. Phys. D Atom. Mol. Cl. **19** (1-4), A11 (1991).

[65] R. B. K. Jena P., Khanna S. N., *Physics and Chemistry of Finite Systems: From Clusters to Crystalls*. (Kluwer, Dordrecht, 1992).

[66] L. S. Bartell, Ann. Rev. Phys. Chem. **49**, 43 (1998).

[67] R. S. Berry, T. L. Beck, H. L. Davis, and J. Jellinek, Adv. Chem. Phys. **70**, 75 (1988).

[68] R. S. Berry and B. M. Smirnov, Physics-Uspekhi **48** (4), 345 (2005).

[69] M. R. Hoare and P. Pal, Adv. Phys. **20** (84), 161 (1971).

[70] J. A. Northby, J. Chem. Phys. **87** (10), 6166 (1987).

[71] J. Xie, J. A. Northby, D. L. Freeman, and J. D. Doll, J. Chem. Phys. **91** (1), 612 (1989).

[72] L. Van Hove, Physica **15**, 951 (1949).

[73] N. Goldenfeld, *Lectures on Phase Transitions and the Renormalization Group*. (Addison-Wesley, Reading, MA, 1992).

[74] H. L. Davis, J. Jellinek, and R. S. Berry, J. Chem. Phys. **86** (11), 6456 (1987).

[75] C. Predescu, (private communication).

[76] I. F. Silvera and V. V. Goldman, J. Chem. Phys. **69**, 4209 (1978).

[77] D. J. Scharf, G. J. Martyna, and M. L. Klein, Low Temp. Phys. **19**, 364 (1993).

[78] A. Calhoun, M. Pavese, and G. A. Voth, Chem. Phys. Lett. **262** (3-4), 415 (1996).

[79] T. D. Hone and G. A. Voth, J. Chem. Phys. **121** (13), 6412 (2004).

[80] S. Habershon, B. J. Braams, and D. E. Manolopoulos, J. Chem. Phys. (submitted).

[81] B. J. Braams, T. F. Miller, and D. E. Manolopoulos, Chem. Phys. Lett. **418** (1-3), 179 (2006).

[82] A. Nakayama and N. Makri, J. Chem. Phys. **125** (2), 024503 (2006).

[83] B. J. Ka, Q. Shi, and E. Geva, J. Phys. Chem. A **109** (25), 5527 (2005).

[84] B. J. Ka and E. Geva, J. Phys. Chem. A **110** (31), 9555 (2006).

[85] I. Navrotskaya and E. Geva, J. Phys. Chem. A **111** (3), 460 (2007).

Tables

Table. 1 Parameters of the Silvera-Goldman potential for *para*-hydrogen

α 1.713	C_6 12.14
β 1.5671	C_8 215.2
γ 0.00993	C_9 143.1
r_c 8.32	C_{10} 4813.9

Table. 2 Average kinetic energy per molecule (divided by k_B) of liquid *para*-hydrogen at $T = 25$ K, $\upsilon = 31.7$ cm^{3}mol^{-1} and $T = 14$ K; $\upsilon = 25.6$ cm^{3}mol^{-1} under nearly zero extent pressure (the statistical error of the TGA is less than 0.1 K)

Temperature (K)	Average kinetic energy per molecule (K)					
	Full-TGA Kubo	SP-TGA Kubo	RPMD[55]	FK-LPI[43]	PIMC[54]	classical
25	64.5	64.5	64.3	61.3 ± 1.2	61.9	37.5
14	65.0	65.6	67.7	…	63.2	21

Table. 3 Diffusion contants for liquid *para*-hydrogen at $T = 25$ K, $\upsilon = 31.7$ cm^{3}mol^{-1} and $T = 14$ K; $\upsilon = 25.6$ cm^{3}mol^{-1} under nearly zero extent pressure

			Diffusion constant (Å^2/ps)	
		N	25 K	14 K
Experiment[51]			1.6	0.4
LSC-IVR	Full-TGA	108	1.81 ± 0.02	0.63 ± 0.01
	SP-TGA	108	1.84 ± 0.02	0.65 ± 0.01
FK-LPI[43]		125	1.73	…
FBSD[54]		108	1.68 ± 0.05	0.75 ± 0.07
CMD[56]		216	1.50	0.32
RPMD[55]		Linearly extroplated to ∞	1.59 ± 0.01	0.33 ± 0.01
RPMD+MEAC[80]		256	1.78	0.41
MEAC[53]		108	1.47	0.28
QMCT[52]		108	1.69	0.30
Classical[55]		Linearly extroplated to ∞	0.56 ± 0.02	0.02 ± 0.01

Figure Captions

Fig. 1 (Color online). Average energy per particle of the Ne_{13} LJ cluster system. Solid line: the path integral Monte Carlo (PIMC) result. Circles with solid line: the fully thermal Gaussian approximation (Full-TGA) result. Triangles with dashed line: the Classical Monte Carlo (CMC) result.

Fig. 2 (Color online). The Kubo-transformed force autocorrelation function per particle for the Ne_{13} LJ cluster system. Solid line: the classical result. Dotted line: the TGA-LSC-IVR result. Temperature in three panels are respectively: (a) $T = 14$ K ; (b) $T = 8$ K ; and (c) $T = 4$ K .

Fig. 3 (Color online). The Kubo-transformed momentum autocorrelation function per particle (divided by $2mk_B$) for the liquid *para*-H_2 at two state points: (a) $T = 25\ \text{K}, \upsilon = 31.7\ \text{cm}^3\text{mol}^{-1}$ and (b) $T = 14\ \text{K}; \upsilon = 25.6\ \text{cm}^3\text{mol}^{-1}$. Solid line: the LSC-IVR result with the Full-TGA. Dashed line: the LSC-IVR result with the SP-TGA. Dot-dashed line: the RPMD result[80]. Dotted line: the RPMD+MEAC result[80].

Fig. 4 (Color online). The normalized symmetrized momentum autocorrelation functions for the liquid *para*-H_2 at the state point $T = 25\ \text{K}, \upsilon = 31.7\ \text{cm}^3\text{mol}^{-1}$. Solid circles: the complex time PIMC results[82]. Solid line: the TGA/LSC-IVR result. Dot-dashed line: the FBSD result[82]. Dotted line: the RPMD result[80]. Long-dashed line: the RPMD+MEAC result[80]. Short-dashed line: the MEAC result[80]. Panel (b) shows a blowup of the curves shown in (a).

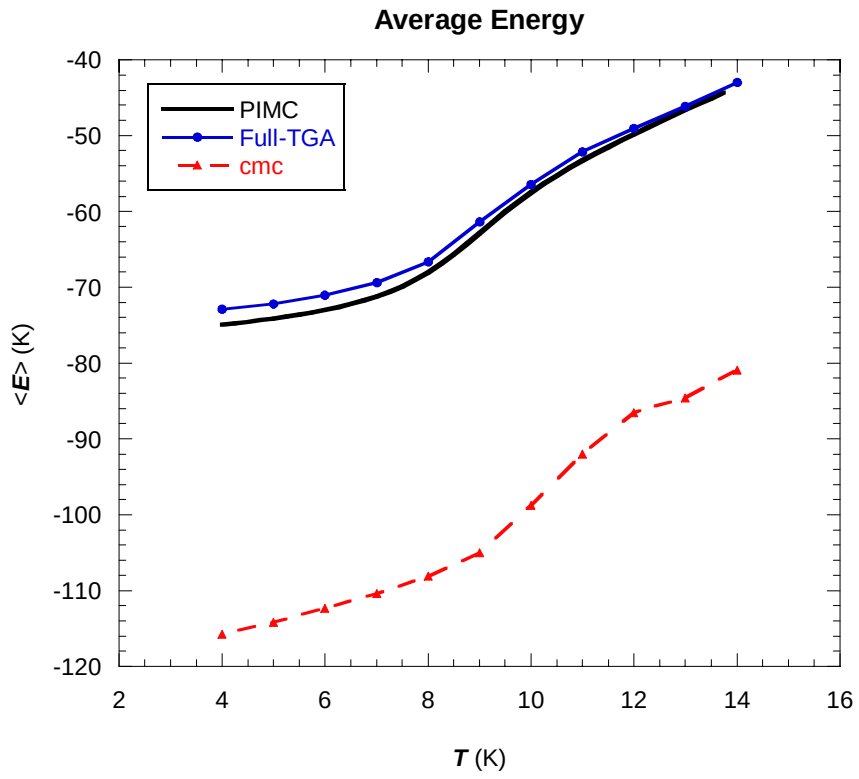
Average Energy
PIMC
Full-TGA
cmc
-40
-50
-60
-70
-80
-90
-100
-110
-120
2
4
6
8
10
12
14
16
<E> (K)
T (K)

Fig. 1

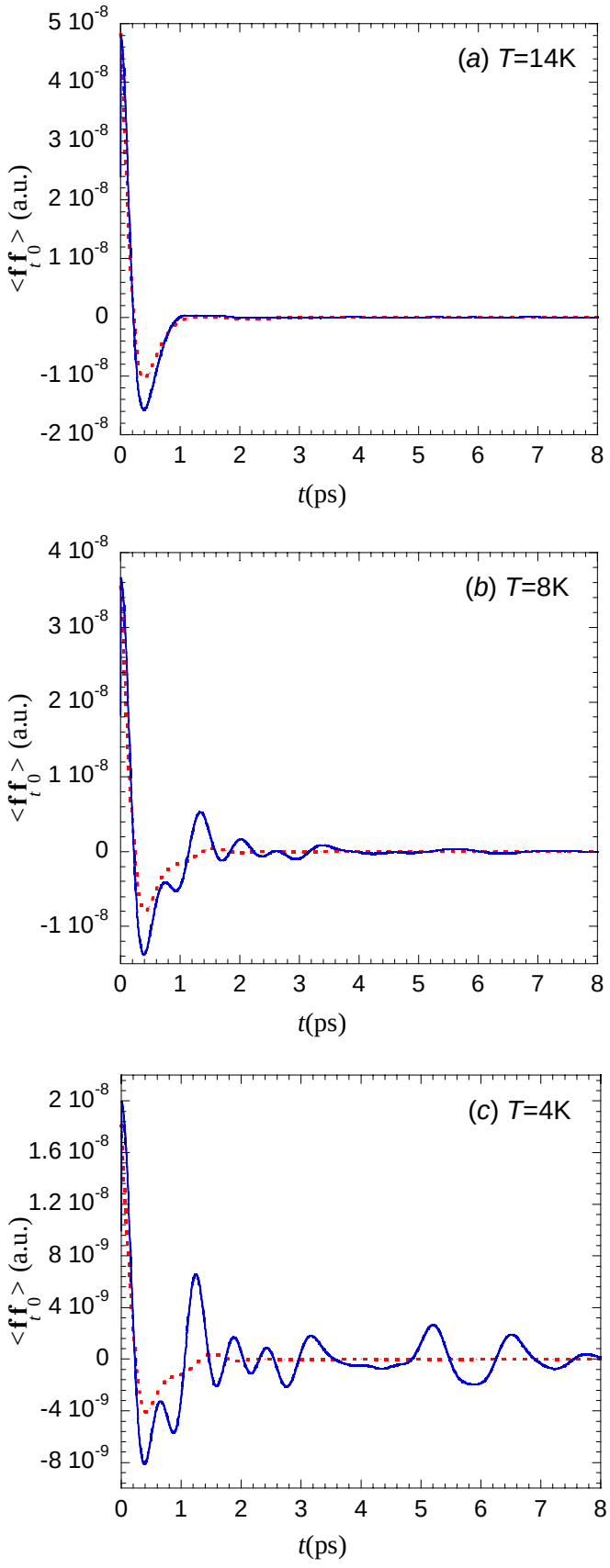

Fig. 2

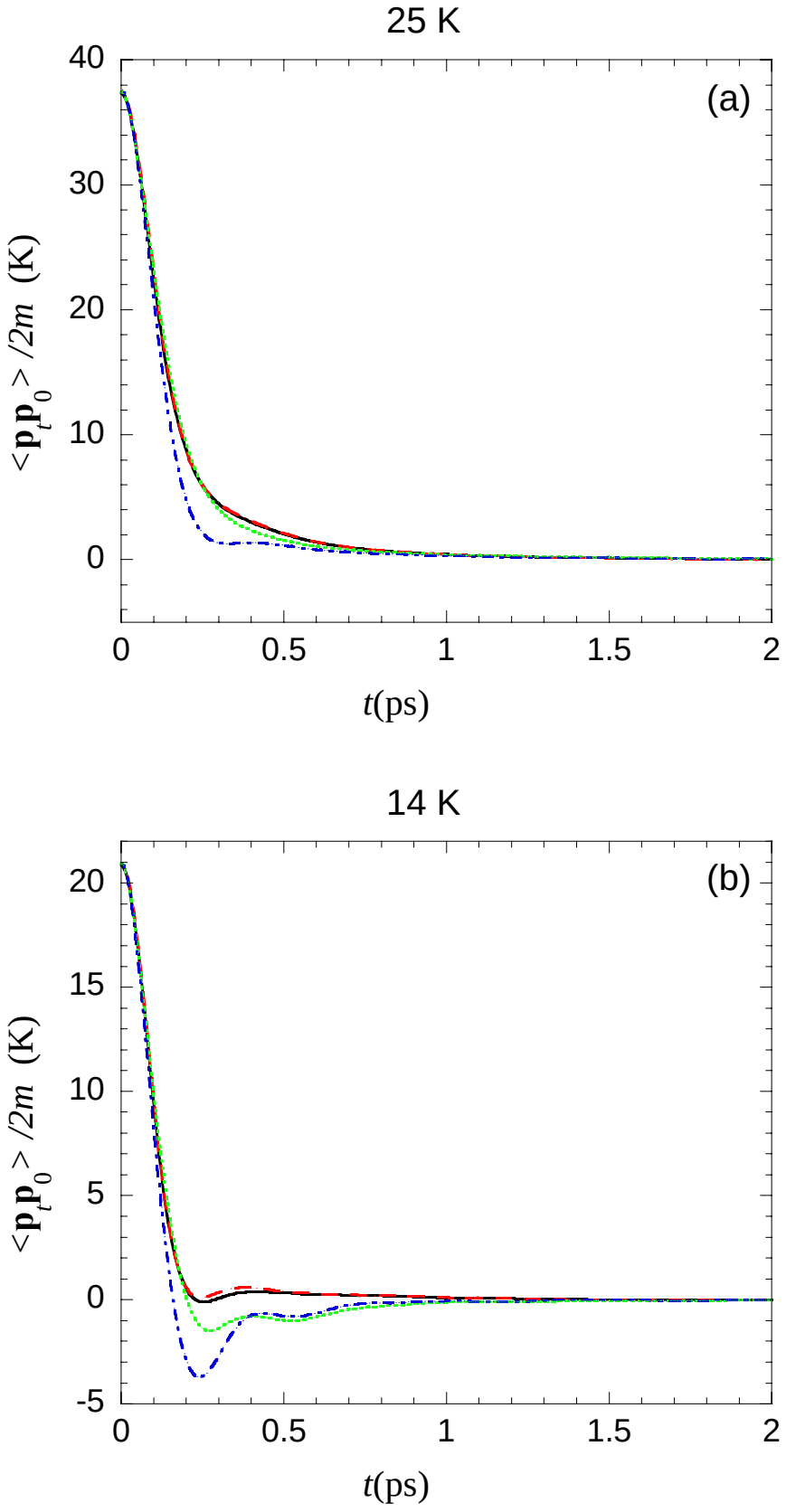
25 K
(a)
40
30
20
10
0
0
0.5
1
1.5
2
t(ps)
$<\mathbf{p}_t\mathbf{p}_0>/2m$ (K)
14 K
(b)
20
15
10
5
0
-5
0
0.5
1
1.5
2
t(ps)
$<\mathbf{p}_t\mathbf{p}_0>/2m$ (K)

Fig. 3

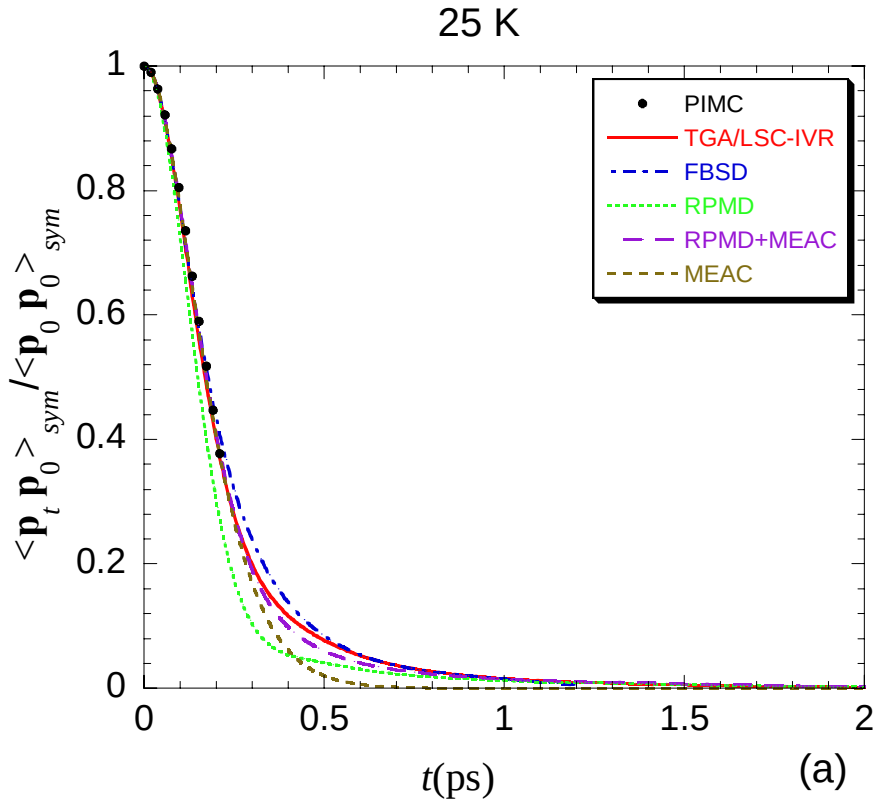
25 K
PIMC
TGA/LSC-IVR
FBSD
RPMD
RPMD+MEAC
MEAC
$<\mathbf{p}_t\,\mathbf{p}_0>_{sym}/<\mathbf{p}_0\,\mathbf{p}_0>_{sym}$
t(ps)
(a)

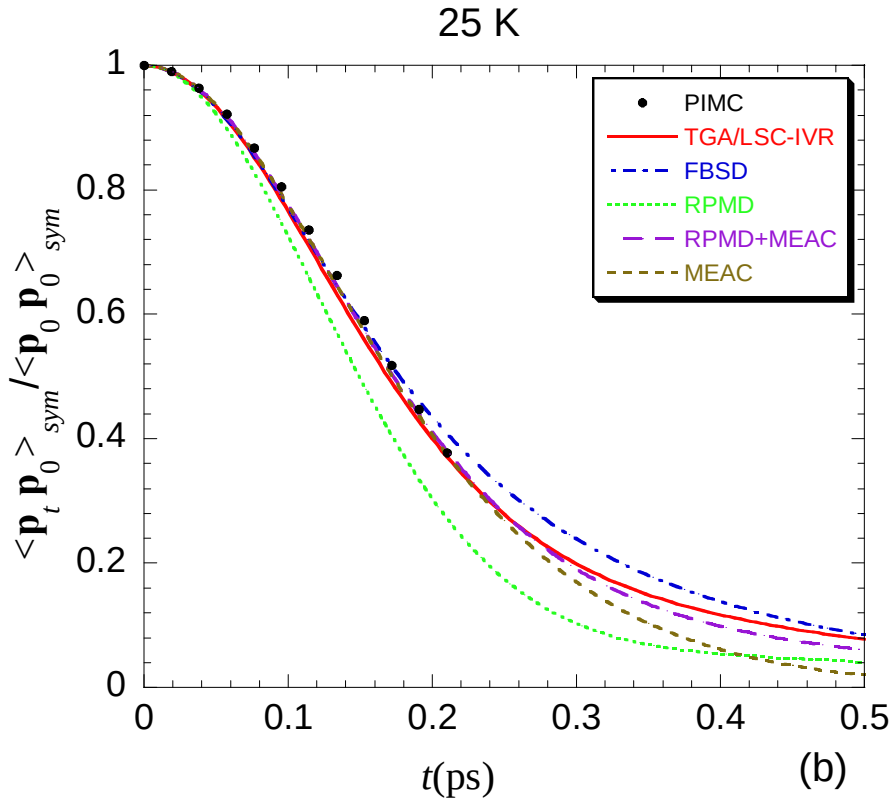
25 K
PIMC
TGA/LSC-IVR
FBSD
RPMD
RPMD+MEAC
MEAC
$<\mathbf{p}_t\,\mathbf{p}_0>_{sym}/<\mathbf{p}_0\,\mathbf{p}_0>_{sym}$
t(ps)
(b)

Fig. 4